Superconducting magnets for Energy Buncher at FAIR

R. K. Bhandari*, M. Ahammed, P. Bhattacharya, S. Bhattacharya, S. Chattopadhyay, T. K. Bhattacharya, U. Bhunia, J. Chaudhuri, M. K. Dey, A. Dutta, A. DuttaGupta, C. Mallik, B. Mandal, B. Manna, C. Nandi, G. Pal, S. Roy, S. Saha and P. R. Sarma

Variable Energy Cyclotron Centre, 1/AF, Salt Lake, Bidhan Nagar, Kolkata 700 064, India

A set of large superconducting magnets have been designed for the Low Energy Buncher (LEB) of the Superconducting Fragment Separator (Super-FRS) for FAIR. The set of magnets will include dipoles and multipoles (sextupole and quadrupole) of stringent quality criteria. Details of design and expected performance have been discussed.

Keywords: Energy Buncher, FAIR, purcel filter, magnets.

Introduction

THE Energy Buncher at the low energy beamline of the superconducting fragment separator (Super-FRS) (Figure 1) at FAIR is a valuable and attractive experimental device for particle identification after secondary reactions[1]. This device will be at the heart of the experimental facility for nuclear and reaction (NuSTAR) studies using radioactive ion beams at FAIR. The dipole, quadrupole and sextupole magnets forming the Energy Buncher have to accept fragment beams which can be transported in a large cylindrical volume. The unique feature of FAIR is the high beam intensity coupled with the ability to change the beam energy and beam species at short interval of time. The magnets, therefore, have stringent design criteria. The dipole magnets have large usable aperture of ± 380 mm horizontally and ± 100 mm vertically with maximum magnetic field intensity 1.6 T with uniformity 3×10^{-4}. The quadrupole magnets have large usable aperture of ± 300 mm horizontally and ± 250 mm vertically with maximum magnetic field intensity 1.8 T with field quality gradient ($\Delta G/G$) of 8×10^{-4}.

Preliminary calculations show that the required magnetic field and field gradients can be reached both by normal room temperature magnets and superconducting magnets. If we use copper conductor operating at room temperature, the size of the coil becomes large and the length of the pole stem has to be about the same as the half-aperture of the magnet. As a result, the magnet yoke will have large cross-section. So the cost of copper will be about the same as that of iron. A feasible alternative is to adopt superferric magnet technology. In a superferric magnet, the coil size is very small and the iron volume also is large. The field is iron dominated, though the coil is superconducting. Superferric magnets have the combined advantage of a very compact coil and low operating cost. The superferric magnet technology has been adopted at various laboratories like MSU, A1900 fragment separator[2], RIKEN, BigRIPS fragment separator[3], in-flight separator for RIA[4] in USA, etc.[5–7]. All of these facilities work at lower beam energies and hence the magnets are much smaller compared to those of the Super-FRS.

As a constituent member of FAIR, India is seriously considering a proposal to supply hardware for building this accelerator facility. It is indeed a privilege and technological challenge for India to design superconducting magnets for use at FAIR. The experience by Indian scientific community in building the superconducting cyclotron at VECC-Kolkata and other superconducting devices will provide necessary knowhow for this project. The project itself is, however, unique in terms of the size of the magnets, and has stringent requirement in addition to building a large number of them with guaranteed quality control.

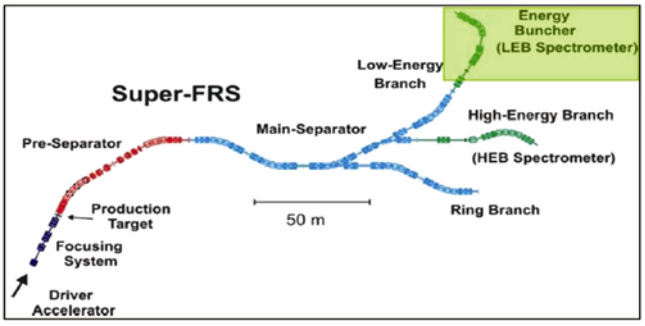

Figure 1. Layout of Super-FRS with Energy Buncher shown by shaded region.

*For correspondence. (e-mail: bhandari@vecc.gov.in)

The superconducting magnets will use Nb–Ti conductors. Nb–Ti has a characteristic property of offering no resistance to the flow of electricity when cooled below a critical temperature. So, it is required to immerse the coil in a liquid helium bath. The 4.5 K helium chamber is completely covered with a thermal shield cooled by helium at 50–80 K on its outer and inner surface. The helium chamber and thermal shield are enclosed in a vacuum shell.

Superconducting dipoles

The superferric dipoles will have radius of curvature of 4.375 m, magnetic field up to 1.6 T with a field uniformity better than $\pm 3 \times 10^{-4}$ over elliptical bore of size ± 380 mm $\times \pm 100$ mm and effective length 1.708 m to bend ion beams by an angle 22.5°. This magnet system consists of mainly two sub-systems, i.e. cryostat and iron yoke. The present status of the design of the dipoles as is being carried out at VECC-Kolkata is given below. Specifications of the dipole magnet are given in Table 1.

Preliminary 2D magnetic field analysis has been carried out using POISSON code and results are represented as a plot of magnetic field uniformity versus radial distance for various excitation as shown in Figure 2. It is observed that maximum field achieved is 1.6 T at 227 A excitation. Field uniformity achieved is better than 1.5×10^{-4}. During analysis, it is revealed that employing purcel filter would enhance the field uniformity significantly.

Figure 3 shows the sensitivity of the field uniformity with the number and shape of purcels. It is seen that a cross-shaped purcel is more effective than rectangular shape, though from the fabrication point of view rectangular purcels are preferred to crossed ones.

After achieving the desired magnetic field uniformity in the 2D calculation, 3D field analysis has been carried out using MagNet and TOSCA[8,9].

First 3D analysis has been carried out using the D-shaped coil and iron pole instead of C-type to avoid the difficult coil winding process in the concave surface of the bobbin. With some minor modifications of the iron, the desired field has been achieved. Purcels used in the 3D analysis were in the shape of a circular arc which is rather difficult to fabricate. Therefore efforts are on to achieve the field uniformity in 3D analysis using the straight coil, pole chamfering and cross-shaped purcel filter. Cross-shaped purcel filters have been found to give better uniformity than rectangular filters. A cross-shape

Table 1. Specifications of the dipole magnet

Maximum/minimum field	1.6/0.15 T
Bending angle/no. of magnets	22.5°/4
Radius of curvature	4.375 m
Effective length	1.708 m
Usable horizontal aperture	± 380 mm
Usable vertical gap	± 100 mm
Vertical pole gap	± 120 mm
Field quality	$\pm 3 \times 10^{-4}$
Pole face rotation	0°

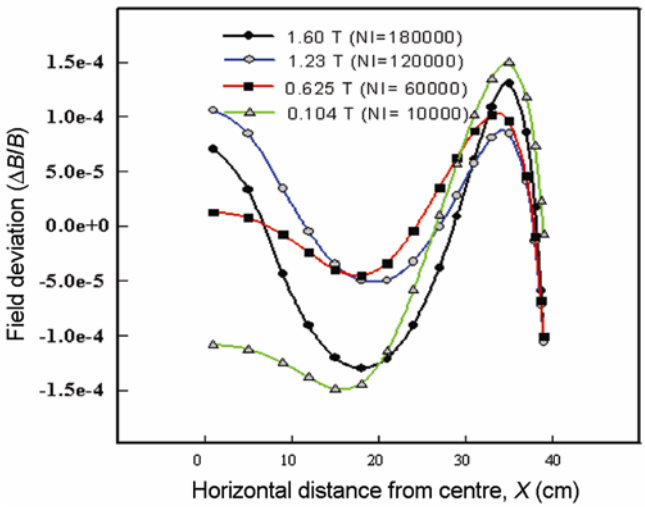

Figure 2. Uniformity of the magnetic field with radial distance for a configuration with parcel filter.

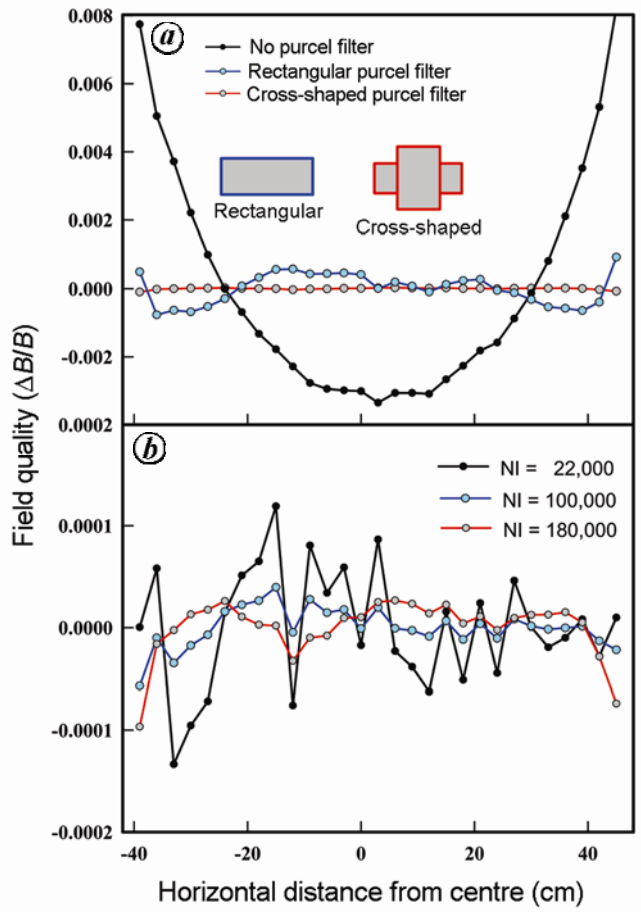

Figure 3. ***a***, Field quality with various purcel filters. ***b***, Field quality for different excitations with a cross-shaped purcel filter.

has more number of parameters which can be optimized for getting better uniformity. A field uniformity of 5×10^{-4} over required aperture of ± 380 mm and ± 100 mm has been obtained. The dimension of the magnet for this field uniformity is $2.2\ \text{m} \times 2.9\ \text{m} \times 1.9\ \text{m}$ and weight is 66 tonnes.

A new idea has been proposed where inserting an iron rod sandwiched between aluminium pieces as shown in Figure 4 within the cylindrical purcel and rotating the rod by any external means, field uniformity could be varied even while keeping the magnet in energized condition. Practical realization of the idea could avoid the time consuming and tedious method of post-magnetic field measurement shimming process.

Based on the available preliminary magnetic field design data, a conceptual design of the cryostat is completed as shown in Figure 5. As the precision magnetic field analysis is going on, related modification and incorporation of the magnet and cryostat are under progress.

The cable is rectangular ($2.24\ \text{mm} \times 1.43\ \text{mm}$) shape having Nb–Ti filaments embedded in copper matrix. This is readily available from M/s Oxford Company, UK. Number of turns used is 36 (horizontal) × 22 (vertical).

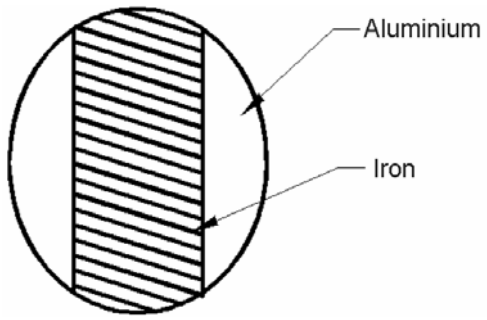

Figure 4. Arrangement of a cylindrical rod.

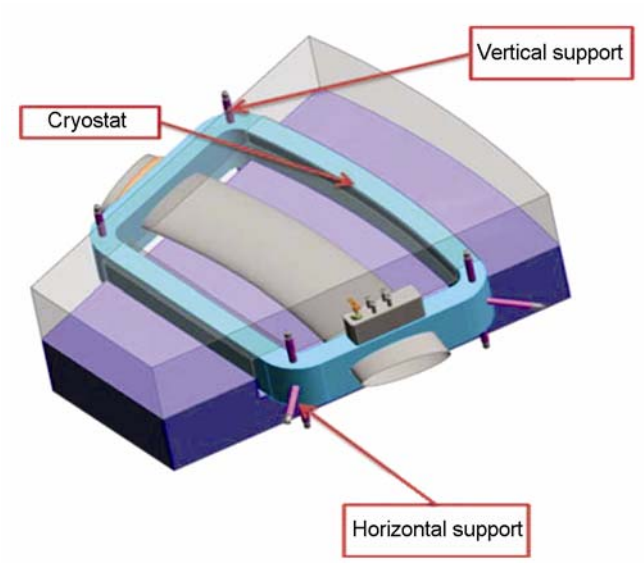

Figure 5. Design of cryostat for dipole.

Different operating conditions are considered for detailed stress analysis of the superconducting coil and helium chamber using ANSYS[10] finite element code. A suitable support design is in process so that excessive deformation of the coil could be avoided. Cracking of the potted coil due to the tensile stress is to be restricted to debar the occurrence of the premature quench of the magnet. Deformation pattern due to Lorentz is shown in Figure 6.

Supports for the helium chamber were designed and optimized for ensuring minimum possible heat leak to the helium chamber and for correct alignments of the superconducting coil. Quench analysis for designing quench circuit along with the selection of fast and slow dump resistance is in progress. Design of the field mapping fixture is currently being initiated.

Superconducting quadrupole and sextupole magnets

The quadrupole and sextupole magnets in the Energy Buncher section of the Super-FRS have to generate high-magnetic field in the usable aperture. Two types of quadrupoles, long quadrupoles with an effective length of 1.2 m and short quadrupoles with an effective length of 0.8 m, are used in the Energy Buncher. The range of magnetic field gradient is also large, from a minimum gradient of 0.05 T/m to a maximum gradient of 4.7 T/m for the short quadrupole. The corresponding figures for the long quadrupole are 0.1 T/m and 5.2 T/m respectively. A field gradient quality $\Delta G/G$ of $\pm 8 \times 10^{-4}$ has to be achieved over a radial aperture of ± 300 mm. The sextupoles have an effective length of 0.8 m, maximum hexapole component of $15\ \text{T/m}^2$ and a field quality of about $\pm 1.5 \times 10^{-3}$. These magnets are required for handling beams with a maximum beam rigidity of 7 T/m.

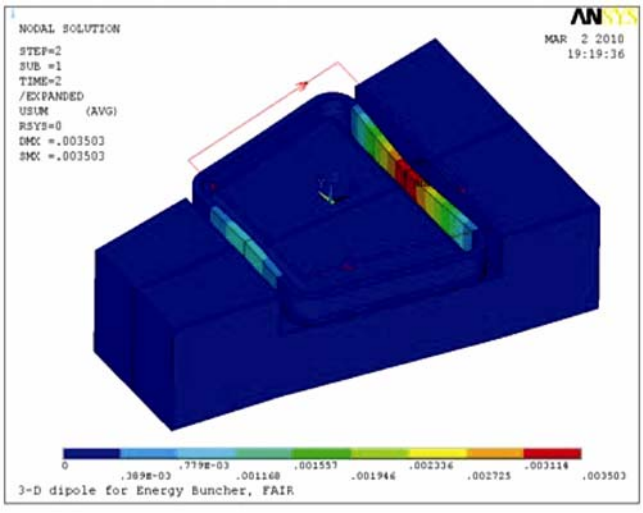

Figure 6. Deformation pattern of the coil due to Lorentz force.

These are DC magnets, but there is a need of frequent change in field level from experiment to experiment. Quick changes in the field levels are needed for increasing the usable beam time. A ramp rate of 120 s has been thought to be optimum for this changeover. Laminated iron core will be utilized for minimizing the eddy loss, which occurs due to the fast change of operating current.

A 2D design of the quadrupole was performed using a small superconducting coil to work out the approximate size of the magnet. The cross-section of the coil used is 100 mm × 43 mm. The current density is 110 A/mm^2. Figure 7 shows the 2D design of the magnet with equipotential lines.

Material data for low carbon steel has been used for the analysis. The results show that the maximum field gradient is 5.2 T/m, pole tip field is 1.7 T and yoke field is 2 T. Based on the approximate magnet design, the layout of the quadrupole magnet and coil has been worked out as shown in Figure 8.

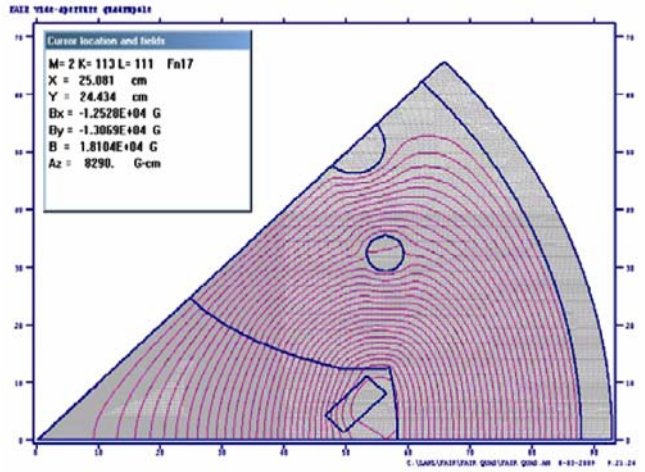

Figure 7. 2D design of the quadrupole.

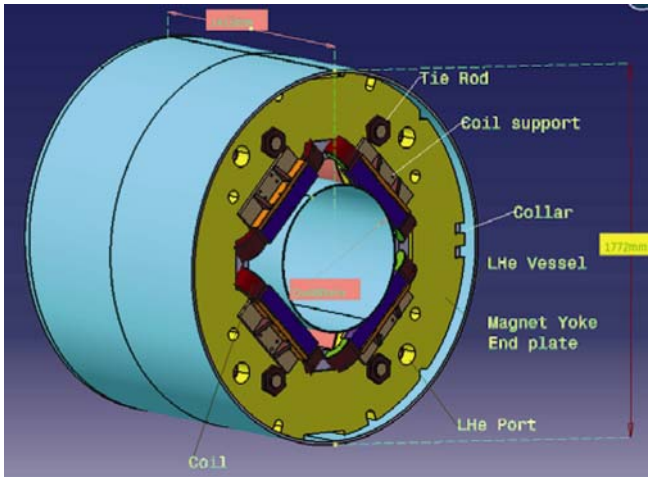

Figure 8. Quadrupole liquid helium chamber.

The 3D magnet design of the quadrupole and sextupole was performed using the code MagNet[8] on a one-eighth symmetry and half length quadrupole model (Figure 9) and a one-twelfth symmetry and half length sextupole model (Figure 10).

The super conductor used for quadrupole and sextupole is same as dipole with an operating current of about 300 A. The coil will produce 290,000 A-turns. The Nb–Ti conductor is embedded in a copper substrate for giving high Cu/SC ratio to ensure cryogenic stability of the coil. The field pattern obtained from the 3D design matched closely with the 2D design. However, because of the short length and large usable diameter, large end effects were observed. A number of iterations involving increasing the ampere-turn and selective removal of material from the pole edge were required to design the magnet end chamfer and achieve the required field quality.

It was observed that the quadrupole magnet could be designed for field gradient quality better than 8×10^{-4} and the sextupole magnet could be designed for field quality better than 1.5×10^{-3}. Figures 11 and 12 show the achieved field quality for quadrupole and sextupole for different excitations.

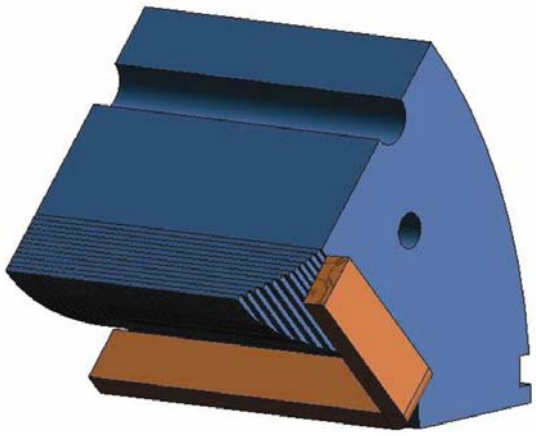

Figure 9. One-eighth and half-length symmetry model.

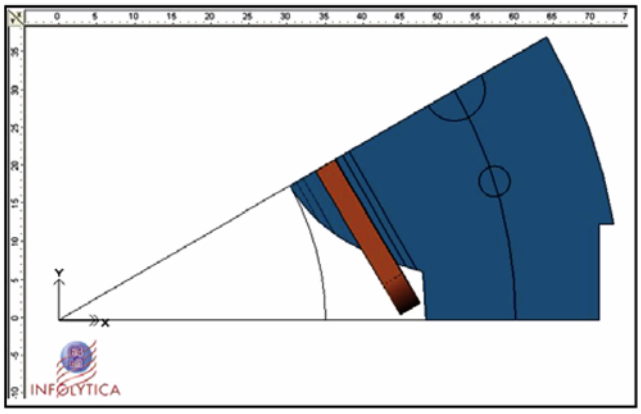

Figure 10. One-twelfth and half length symmetry sextuple model.

In an ideal quadrupole, the transverse magnetic field intensity is proportional to the distance r from the axis of the magnet[11]. Higher order multipoles affect this radial field dependence and leads to geometrical aberrations. In general, then, one wants to minimize the contributions of these higher order multipoles to the field. Computer code OPERA 3D was used to minimize the harmonics. The modified end profile is given in Figure 13. The minimized harmonics for maximum and minimum excitations at the reference radius of 300 mm are shown in Figure 14 *a* and *b* respectively. It is highly dependent on the end chamfer profile.

The magnet iron and coil are immersed in liquid helium inside the liquid helium chamber. Stainless steel of type SS304 has ferrite content in the weld zone, so a fully austenite grade of stainless steel, SS316, has to be used.

The magnet is assembled at room temperature. But it is operated at a temperature of about 4.5 K. Iron contracts by about 2.3 mm for a metre and stainless steel contracts by about 3 mm in a metre when cooled down from room temperature to 4.5 K. The contraction of iron changes the pole profile of the magnet. It is observed that the iron is deformed by about 0.8 mm due to the cool down (Figure 15). In order to keep the magnet quality within acceptable limits, the distortion in iron profile should be less than 50 micron. This required re-evaluation of the iron profile at room temperature. The pole face geometry at room temperature was evaluated in an iterative process by successively correcting the pole face geometry for deviations. Also as stainless steel contracts more than iron, it applies an external force on the iron to the order of 3.8 MPa.

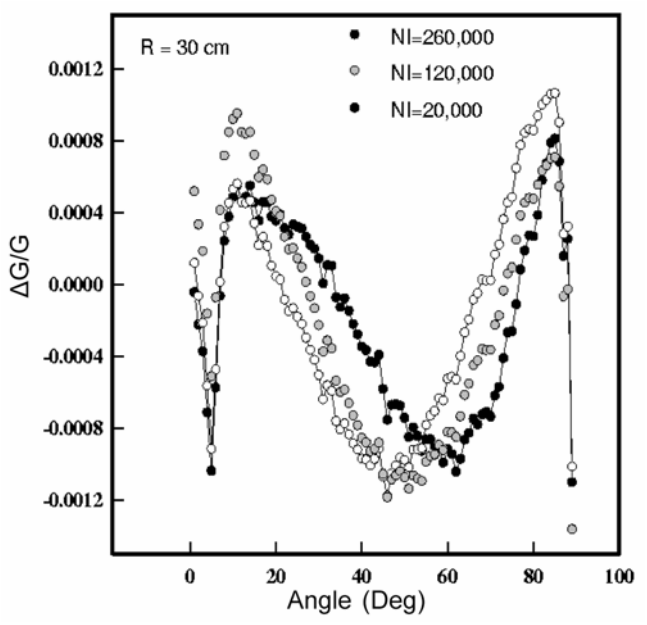

Figure 11. Field gradient quality of the long quadrupole for Energy Buncher–Pole champhered as shown in quadlong_champhered.JP and field deviation at constant radius – 3D calculation.

The Nb–Ti superconductor is wound on a SS316 bobbin and potted with resin to fill the voids to provide strength to the coil and prevent conductor movement during energization of the coil due to Lorentz forces. Resisting conductor movement in the coil is important in a superconducting coil. The assembly of coils and bobbin is mounted on the iron around the pole tip using a fixture made of SS304. The magnitude and direction of forces on the coil were evaluated using computer code OPERA[9]. The maximum deviation of iron was observed to be below 0.1 mm during energization. The overall stress contour in the iron of the quadrupole, coil and coil supports due to the energization forces is given in Figure 16 *a* and *b* respectively. It is observed that the maximum stress in iron and coil is about 38 MPa and 314 MPa respectively. The coil supports need to be modified and modelled using advanced contact elements to re-evaluate coil stress.

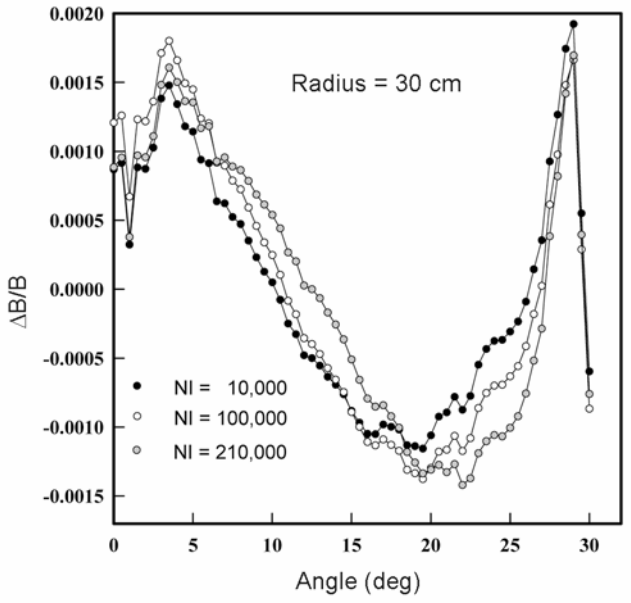

Figure 12. Field quality of the sextupole.

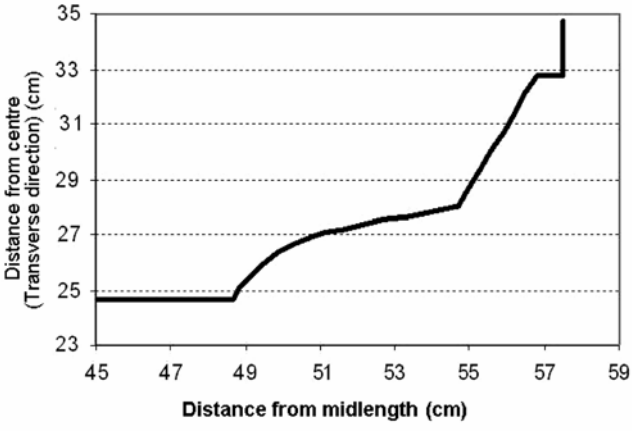

Figure 13. Shape of the end chamfer.

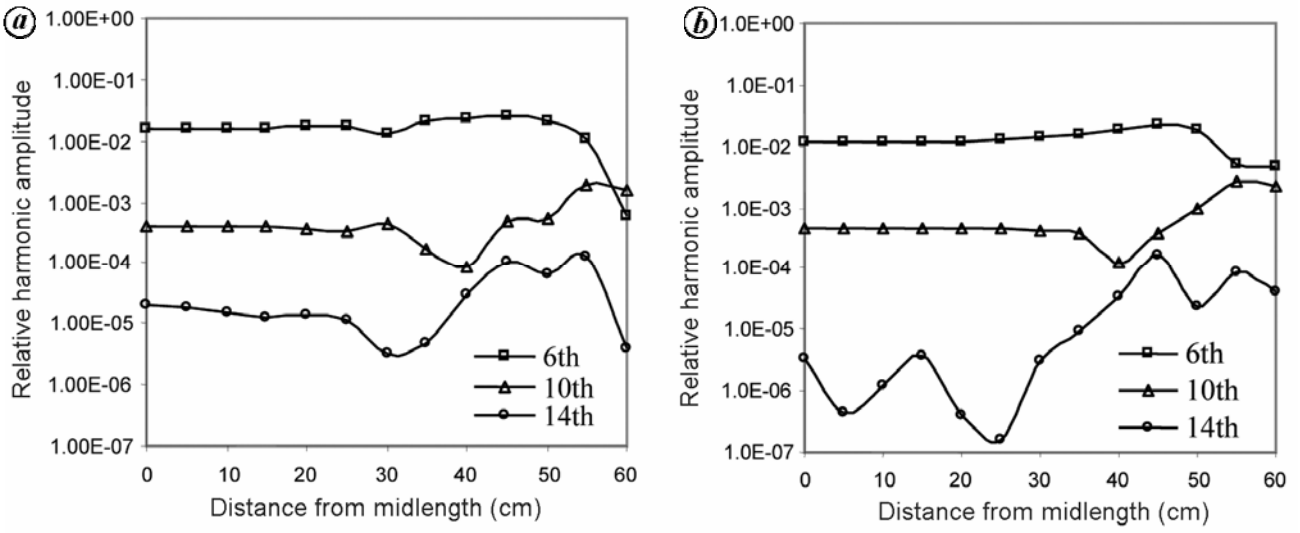

Figure 14. Higher order harmonics along the length of the quadrupole at (***a***) maximum excitation and (***b***) minimum excitation.

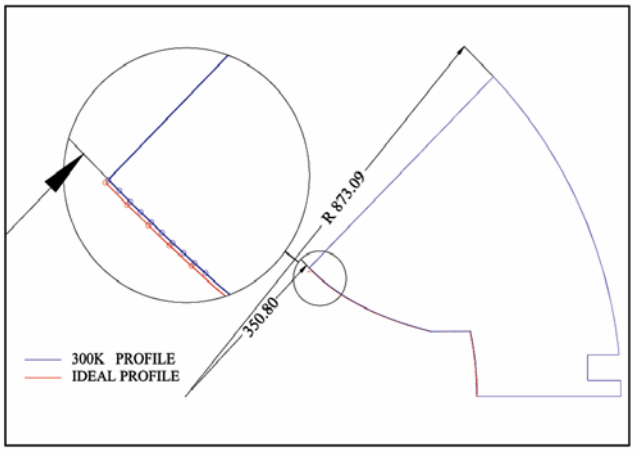

Figure 15. Geometry of quadrupole iron after cool down.

The coil and iron are completely immersed in liquid helium in the liquid helium chamber. The 4.5 K helium chamber is completely covered with a thermal shield cooled by helium at 50–80 K on its outer and inner surface. The helium chamber and thermal shield are enclosed in a vacuum shell. In order to operate the magnets efficiently, the design of a cryostat has to be structurally optimum. Reduction of heat transfer to the cryogenic fluid contained in the cryostat is one of the prime considerations in designing the magnet. Radiation, convection and conduction mode of heat transfer are involved in the process of heat transfer. The liquid helium chamber is placed in a vacuum vessel, eliminating the contribution of convection. Radiation is reduced by applying layers of highly reflective media on the liquid helium and 80 K shield. All the supports and connectors have to be properly designed to reduce conduction heat leak. A rough estimate shows that the heat leak to the liquid helium system is about 10 W at 4.5 K.

As a part of the design study from the point of view of safety, we considered two main aspects during design of the superconducting magnet: quench of the magnet and sudden vacuum break of the cryostat annulus vacuum by air. The worst scenario will occur, if both the processes occur at the same time.

Quench is the phenomenon where a part of the superconducting coil becomes a normal conductor due to a small energy release and consequent rise in temperature above its critical temperature[12]. The OPERA-QUENCH software has been used for the quench study of the quadrupole coils. Four epoxy impregnated coils of the quadrupole are connected in the series. The coils are connected to the power supply via a circuit breaker. A protection resistance is connected in parallel across the coils. Though the coils are in a pool of liquid helium, during the quench analysis, it is assumed that the coils are adiabatic, i.e. during the quench propagation, heat is not transferred to liquid helium from the coil. This is a good assumption as the coils are epoxy impregnated and typical quench duration is very small. In the analysis, quench is initiated by placing a foil heater on the coil surface. As the quench zone propagates along the conductor, its resistance and also voltage drop changes with time. Once the quench is detected, the circuit breaker opens and the current flows through the protection resistance enabling release of the stored energy in the dump resistor. The dump resistor has separate provision for cooling.

The quench process and maximum temperature rise depend on the value of protection resistance. Higher resistance value shall dump the energy faster. So, temperature rise will be less, but in that case, potential drop across the resistance shall be higher and circuit breaker

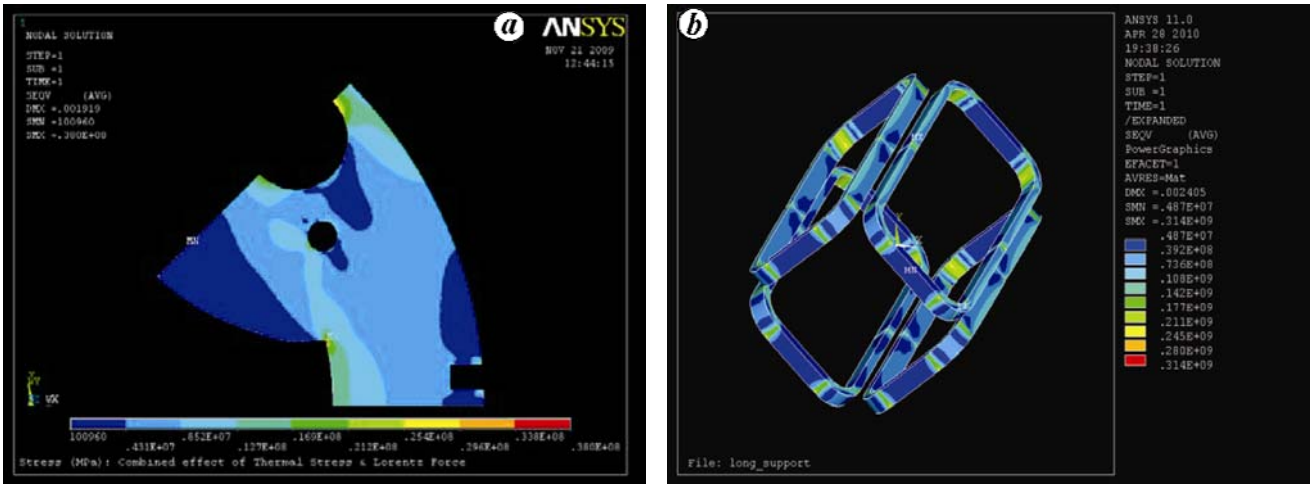

Figure 16. Stress in quadrupole magnet iron at 300 A (***a***) and quadrupole coil at 300 A (***b***).

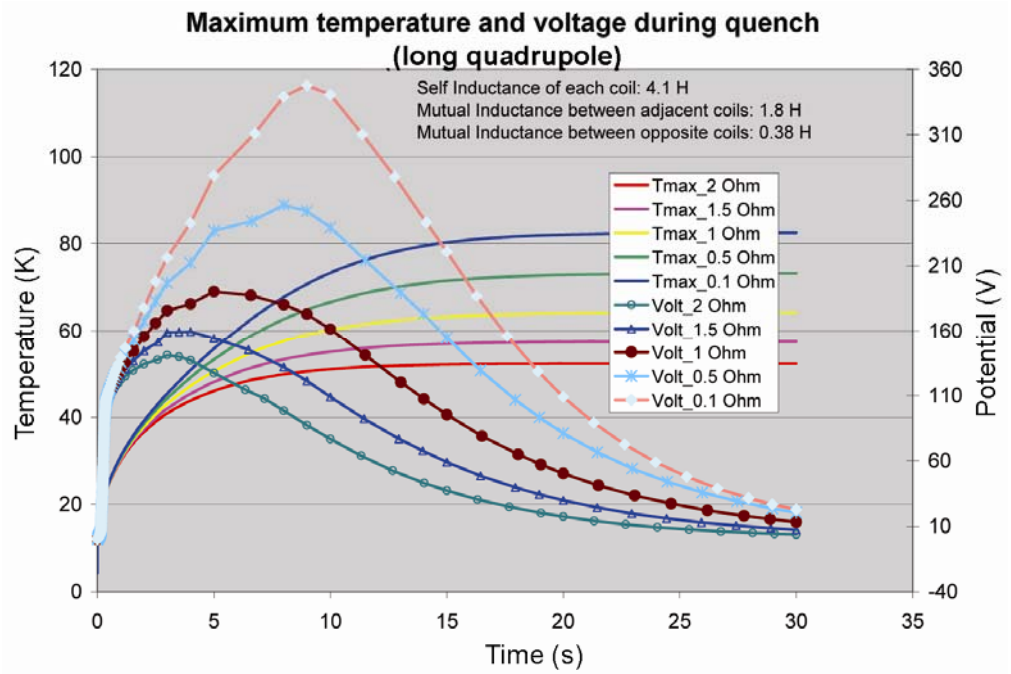

Figure 17. Temperature rise and potential during quench.

and other components in the electrical circuit must be capable of withstanding the consequent voltage. Figure 17 gives the temperature rise and potential developed in the coil during quench of a quadrupole magnet. For the safety of cryostat, it is assumed that all coils are quenched at a time and protection resistance is very low. So, all energy is dissipated to four coils and, thereafter, heat dissipation rate to liquid helium will be maximum. Heat dissipation rate shall depend on the surface temperature of the coils.

For cryostat safety analysis, equilibrium temperature of the coils after quench is taken as surface temperature and this temperature is assumed to be constant throughout the period of pressure rise in cryostat and venting of helium from the vent port.

Loss of annulus vacuum is another major concern, because it can increase the heat in-leak by several 100 times to liquid helium. In case annular vacuum space suddenly gets vented by atmospheric air, cryostat pressure shall suddenly increase to a very high value due to this heat in-leak. Several interrelated mechanisms occur during this loss of vacuum that affect the heat transfer. Immediately after the vacuum breakdown, air comes in contact with the cold surface. It gets condensed and subsequently solidifies. The layer of ice that is formed on the surface of the liquid helium chamber changes the process

of conduction, convection and radiation heat transfer into liquid helium. The heat transfer coefficients vary rapidly over time as the layer of ice increases. In reality, the phenomenon is not only the condensation, freezing of a pure gas or vapour but a condensation, freezing and melting of several components of air. Available data and correlations for heat transfer coefficients for such type of non-steady state condensation, and freezing and melting of different components of air are insufficient and are of limited accuracy only. Lehman and Zahn[13] had carried out a model experiment on various types of liquid helium standard dewars and cryostats. Maximum heat in-leak rate to liquid helium for LN2 shielded superinsulated helium cryostat was observed to be 0.6 W/cm^2 during that experiment. This heat flux has been used for calculation of total heat load due to loss of vacuum. It was observed that the heat load to the liquid helium system is 144 kW, when quench and loss of vacuum occurs concurrently. A DN80 rapture disc can handle the large amount of helium gas generated due to this heat load to ensure safety of the cryostat.

Summary

In summary, in an effort to build large and unconventional superconducting magnets for the energy buncher at FAIR, optical and preliminary engineering design studies have been carried out. For dipoles, even though 2D design calculations provide desired field quality, 3D calculations, however, show that the field uniformity of 5×10^{-4} could be achieved in place of desired 3×10^{-4}. Various options are being explored to improve the performance. For multipoles however, desired field quality could be achieved in both 2D and 3D calculations. Preliminary design studies for cryostat, support structure, quench analysis and protection mechanism as well as other safety issues have been performed and ready to be validated with a prototype.

1. Technical Report on the Design, Construction, Commissioning and Operation of the Super-FRS at FAIR.
2. Morrissey, D. J. *et al.*, A1900 in-flight fragment spectrometer at MSU. *NIM B*, 1989, **126**, 247.
3. Kubo, T., BigRIPS fragment separator at RIKEN. *NIM B*, 2003, **204**, 97.
4. Sherrill, B., In-flight separators for RIA in USA. *NIM B*, 2003, **204**, 765.
5. Zeller, A. F. *et al.*, Magnetic elements for the A1900 fragment separator. *Adv. Cryogen. Eng. B*, 1998, **43**, 245.
6. Chouhan, S. *et al.*, Design of superferric magnet for the cyclotron gas stopper project at the NSCL. In Proceedings of the Particle Acceleration Conference PAC07 (Albuquerque, 2007), 2007, p. 524.
7. Esser, F. M., Development work for a short, curved superconducting dipole magnet for the HESR at FAIR. EPAC 08, Genoa, Italy.
8. Magnet design code 'MAGNET' from M/s Infolytica.
9. *Opera 3D User Guide for TOSSCA*, Vector Fields Limited, England; www.vectorfields.com
10. ANSYS User Manual, release 12.0.
11. Reigenstreif, E., Focussing with quadrupole, doublets and triplets. In *Focussing with Charged Particles* (ed. Septier, A.), Academic Press, 1967.
12. Wilson, M. N., *Superconducting Magnets*, Oxford University Publication, 1998.
13. Lehmann, W. and Zahn, G., Safety aspects for LHe cryostat and LHe transport containers, ICEC 7, London, 1978.

ACKNOWLEDGEMENTS. We are grateful to several colleagues at VECC and other participating institutions for useful discussions and other helps in carrying out the reported work. Thanks are also due to Prof. V. S. Ramamurthy, Prof. Bikash Sinha, Prof. Sibaji Raha, Dr Praveer Asthana and many other scientists for their encouragements.